Effect of Prefiltering Cutoff Frequency and Scatter and Attenuation Corrections During Normal Database Creation for Statistical Imaging Analysis of the Brain

Hideo Onishi[1], Yuki Matsutake[2], Norikazu Matsutomo[1], Yuji Kai[1], and Hizuru Amijima[3]

[1]Program in Health and Welfare, Graduate School of Comprehensive Scientific Research, Prefectural University of Hiroshima, Hiroshima, Japan; [2]Center for Diagnostic Imaging, Kurume University Hospital, Kurume, Japan; and [3]Department of Nursing, Hyogo University of Health Sciences, Hyogo, Japan

The present study aimed to quantify which image reconstruction conditions for normal databases and patients affect statistical brain function image analysis using an easy *z* score imaging system (eZIS) and 3-dimensional stereotactic surface projections (3D-SSP). **Methods:** We constructed normal databases based on cerebral perfusion SPECT images obtained from 15 healthy individuals. Each normal database was created with the following unique conditions: a variable Butterworth filter cutoff frequency (fc) with and without scatter and attenuation corrections. To simulate patient data, we selected 1 dataset from among those created from the 15 healthy individuals. The simulated patient data were designed to include hypoperfused regions with prespecified volumes. Using 3D-SSP and eZIS, we compared how the above processing conditions affect the distribution of SD in normal database images and the accuracy of detecting specific regions. **Results:** The SD for the SPECT images increased with the fc of the Butterworth filter. The *z* score decreased by 30% for 3D-SSP and by 14% for eZIS, indicating that the prefilter significantly affected *z* scores. The accuracy of detecting the hypoperfused regions was significantly influenced by the fc; 3D-SSP decreased by 7.51%, and eZIS decreased by 55.34%. The detection accuracy with eZIS, which involves a smoothing process, was significantly decreased. The error of the area of hypoperfused regions was minimized when normal database and patient data were both corrected for scatter and attenuation. **Conclusion:** When the reconstruction conditions (fc, scatter correction, and attenuation correction) at normal database creation differed from those at patient data processing, the *z* scores widely underestimated the analytic results because the SD varied according to the reconstruction conditions. The accuracy of brain function image analysis can be improved by considering the reconstruction conditions and correcting for scatter and attenuation on both normal databases and patient data.

Received Jun. 2, 2010; revision accepted Apr. 21, 2011.

For correspondence or reprints contact: Hideo Onishi, Program in Health and Welfare, Graduate School of Comprehensive Scientific Research, Prefectural University of Hiroshima, 1-1 Gakuenmachi, Mihara, Hiroshima, Japan 723-0053.

E-mail: onisi@pu-hiroshima.ac.jp

Published online Jul. 27, 2011.

Key Words: three-dimensional stereotactic surface projections; *z* score; metabolic mapping; cerebral diseases

J Nucl Med Technol 2011; 39:231–236
DOI: 10.2967/jnmt.110.079871

Brain metabolic mapping techniques such as SPECT or PET have enabled the detection of disorders associated with the early stages of various cerebral diseases (*1–3*). These modalities have become popular and have played an important role as early diagnostic tools in the clinical and medical management of Alzheimer dementia (*4–6*). Interpretation of clinical SPECT and PET images often depends primarily on traditional visual assessment.

However, the quality of the information generated from such tomographic images tends to vary according to the experience and subjectivity of the interpreter (*7,8*). To overcome these issues, analysis of brain function images can involve normalization of the overall shape of the brain; that is, the conversion of SPECT or PET images from patients into brain maps that allow pixel-by-pixel comparisons between individuals (*9*). In addition, hypoperfused regions can be objectively identified brain functions that can be statistically evaluated by comparison with a registered database of brain perfusion SPECT images from healthy individuals.

Regions of interest, in which an operator voluntarily selects areas on the basis of a hypothesis and analyzes them, are used in the conventional method of analyzing local accumulation. Among programs used for such an analysis are statistical parametric mapping (SPM; Wellcome Trust Centre for Neuroimaging) and 3-dimensional stereotactic surface projection (3D-SSP; University of Washington) (*10–12*), which was developed as part of a neurologic statistical image analysis program (NEUROSSTAT; University of Washington). The easy *z* score imaging system (eZIS; Fiji Film RI

Pharma Co.) is a statistical image-processing program that uses SPM2 images (*13,14*). The 3D-SSP and eZIS analysis software packages are widely applied.

However, these tools require a normal database of images of healthy brains (*15*). The normal database was defined as the mean and SD of images calculated using the 3D-SSP method from SPECT images of several healthy individuals.

Generally, each institution should create its own normal database, but this would require the recruitment of many healthy individuals, which would be difficult for a single institution. Moreover, the associated ethical aspects (radiation exposure) and economic aspects (cost of examinations, including those using other modalities required for a determination of normal) further reduce the likelihood that individual institutions will develop their own normal database. Accordingly, the only choice is to use a normal database created by others, with the inevitable complications caused by issues such as differences in SPECT system performance between institutions (collimators, radioisotope dose, and scanning method) and in image-processing methods such as image reconstruction and the presence or absence of corrections for scatter and attenuation (*16–19*).

Therefore, the present study aimed to define how *z* scores are affected by image reconstruction conditions during the creation of normal databases and patient data used for eZIS and 3D-SSP analysis. We measured how SD is altered by changes in the cutoff frequency (fc) of the prefilter that is effective for *z* score calculation and by the presence or absence of corrections. We also simulated patient data containing hypoperfused regions of actual prespecified volumes (perfusion defect) and used the data to comparatively determine the accuracy of detecting regions of interest.

MATERIALS AND METHODS

The normal databases were created using cerebral perfusion SPECT images obtained from 15 healthy individuals. Each normal database was generated with a different fc for the prefilter (Butterworth filter). We also constructed normal databases with and without scatter and attenuation correction. One dataset was selected from among those of the 15 healthy individuals as the patient data.

These patient data included hypoperfused regions of prespecified (actual) volumes. We comparatively examined how the processing conditions affected *z* scores for 3D-SSP and eZIS. Global mean values were used for *z* score calculation.

Hardware

A 3-head GCA-9300A SPECT system (Toshiba Co.) was equipped with low-energy, super high resolution fanbeam collimators (half-value width at the center of the SPECT image, 8.6 mm) and a GMS-5500A/PI data processor (Toshiba). Projection data were obtained from each camera in 12 continuous rotations (128×128 matrix for 4 angles of 120° at 2.5 min per angle of rotation) with photopeaks for triple-energy-window scatter correction. The triple-energy-window method is a type of scattering compensation that uses multiple windows. A GMS-5500UI processed all the images (Toshiba). Signal size was determined using an in-house program running on a personal computer with a Windows XP (Microsoft) operating system.

Normal Databases

An intravenous line was placed in the antecubital veins of 15 healthy individuals (8 men and 7 women; mean age, 62.5 ± 5.3 y) before SPECT started. Each participant lay supine with the eyes closed in a dim, quiet room and was intravenously injected with 740 MBq of ^{99m}Tc-hexamethyl propylene amine oxime. Brain SPECT began 10 min afterward using the 3-head camera. The participants were free of somatic, neurologic, or psychiatric disorders according to their medical history and brain MR images. All provided written informed consent to participate in the study according to the guidelines of the Ethics Committee of the Prefectural University of Hiroshima.

Images were reconstructed using a ramp filter for filtered backprojection. We used a Butterworth prefilter to generate the normal database, with the fc changed in 5 steps to 0.40, 0.45, 0.50, 0.55, and 0.60 cycles/cm. Another normal database was then created, with and without scatter and attenuation corrections, with the fc of the Butterworth filter fixed at 0.50 cycles/cm. The triple-energy-window method was used for scatter correction, with the fc of the Butterworth filter fixed at 0.08 cycles/cm for the subwindows (*20,21*). Attenuation was corrected using the iterative Chang method with the attenuation coefficient set at 0.15 cm^{-1}, and the iterative number was 1 (*22,23*).

Simulated Patient Data

We selected from among the normal datasets a single dataset from a healthy 62-y-old individual. The SPECT data from this individual were reconstructed by filtered backprojection and filtered with a Butterworth filter at 0.5 cycles/cm. Chang attenuation correction and scattering correction using the triple-energy-window method were applied to the reconstructed images. These SPECT data were used as patient data.

The patient data included hypoperfused regions with an area of 972 mm^2 (3 slice images) near the left temporal lobe. The hypoperfused decrease rates were 50% relative to the original SPECT count. The projection data (a total of 90 projections in a 128×128 matrix) were created using an in-house program. The patient data SPECT images were reconstructed using the filtered backprojection method without a preprocessing filter.

Statistical Analysis Software

Data were statistically analyzed using the 3D-SSP program, iSSP (version 3.5; Nihon Medi-Physics Co.), and eZIS (version 3). The templates for 3D-SSP and for eZIS were ^{8}F-FDG PET and ^{99m}Tc-hexamethylpropylene-amine oxime SPECT images, respectively. The normal databases and patient data were smoothed for eZIS using a gaussian filter of 12 mm in full width at half maximum. The resulting *z* score images were evaluated using the same

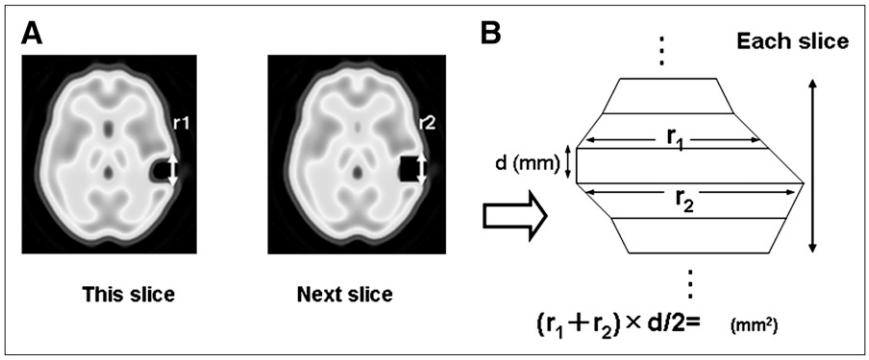

FIGURE 1. Method of determining area of hypoperfused region extracted from patient data to brain surface from area of trapezoidal shape. We calculated distance (r1; mm) of hypoperfused lesion and distance (r2; mm) of next slice using slice thickness (d) in 3 slice images. (A) Distance r1 (mm) measured on surface of nonperfused region in each SPECT slice after anatomic standardization (voxel size, 2.25 mm). (B) Area determined using distances r1 and r2 extracted to brain surface and trapezoidal formula for trapezoidal approximation.

extracted brain surface images for both eZIS analysis and 3D-SSP, which is reliant on brain surface projection.

Evaluation

SD of Normal Databases. Each normal database was generated under a set of unique conditions comprising different fc settings for the Butterworth filter, with and without scatter and attenuation correction. We created SD histograms from SD images of normal databases in each pixel and compared them to determine how discrepancies in image processing conditions affect the SD of the normal databases.

z Score. We defined a 9-pixel-diameter region of interest in the simulated hypoperfused region of brain surface images from which *z* scores were obtained using 3D-SSP and for which eZIS was calculated. We assessed the average *z* scores of the hypoperfused region in the patient data using the normal databases at various fc settings.

Detection Error. We defined a region of interest with the same area as that used for the *z* score appraisal to measure the area of the hypoperfused region. Figure 1 shows the method of calculating the area of the hypoperfused region of the brain surface projection. Error between the measured and actual areas of the prespecified hypoperfused region was determined using the formula below. We similarly calculated the error of the hypoperfused region in patient data and normal database images without corrections. We evaluated how changes in the fc of the normal databases and the presence or absence of scatter and attenuation correction in the normal databases and patient data affected the error in detecting the hypoperfused region.

$$\text{Error} = \frac{(\text{Measured area} - \text{true area of low perfusion region})\ [\text{mm}^2]}{\text{True area of low perfusion region}\ [\text{mm}^2]} \times 100[\%]$$

RESULTS

SD of Normal Databases

Figure 2 shows the results of the SD histogram generated from the normal databases at different fc settings. The average SD obtained by 3D-SSP increased to 0.054, 0.056, 0.064, 0.072, and 0.079 in response to the increases in fc (Fig. 2A). The average SD obtained by eZIS similarly increased to 0.041, 0.044, 0.048, 0.051, and 0.054 (Fig. 2B). The peak SD distribution increased in both analytic methods in response to the increases in fc. The average SD obtained by eZIS remained relatively constant, compared with that obtained by 3D-SSP. The largest increases in the average SDs in 3D-SSP and eZIS in response to changes in fc were 47% and 31%, respectively.

Figure 3 compares SD histograms of normal databases with and without scatter and attenuation correction. The uncorrected average SD was 0.064 for 3D-SSP in Figure 3A, which hardly differed from the attenuation-corrected average SD of 0.062. The peak position of the SD distribu-

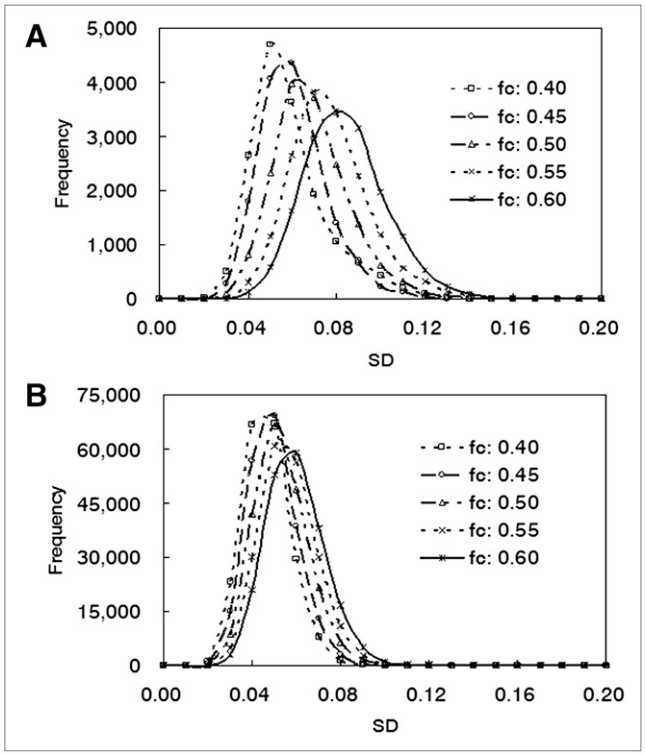

FIGURE 2. 3D-SSP (A) and eZIS (B) histograms of SD in normal database obtained at each fc of Butterworth filter. Histogram distribution of SD was generated from SD of each pixel of brain using data from all participants. Each (3D-SSP, eZIS) histogram for SD scores of normal database was obtained at different fc of Butterworth filter. Horizontal axis is SD score; vertical axis is frequency.

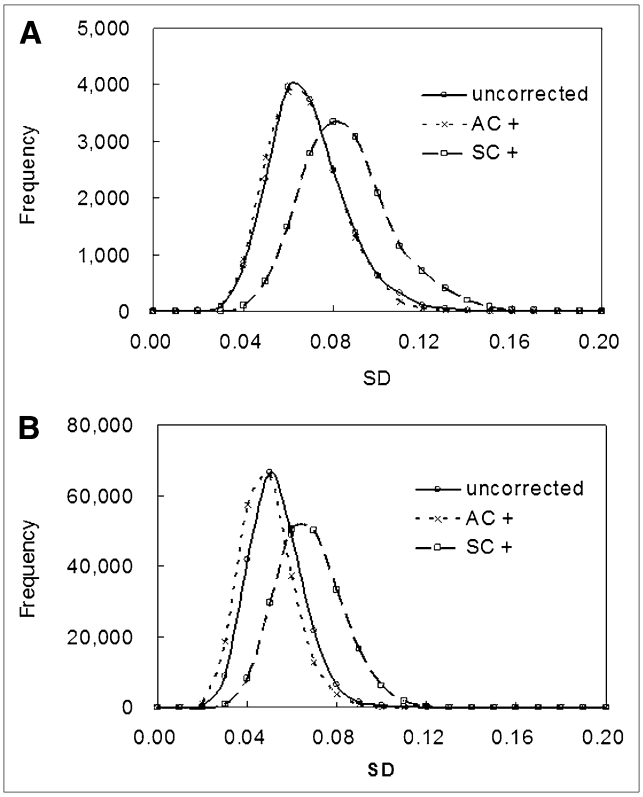

FIGURE 3. 3D-SSP (A) and eZIS (B) histograms of SD in normal database with and without correction. Each histogram of SD scores of normal database was obtained with and without scatter and attenuation correction. Horizontal axis is SD score; vertical axis is frequency. AC+ = with attenuation correction; SC+ = with scatter correction.

tion remained almost constant regardless of attenuation correction. However, the scatter-corrected average SD was 0.081, and the peak position of the SD distribution increased in response to increases in fc. The tendency was the same for eZIS in Figure 3B.

z Score

Table 1 shows *z* scores at various fc settings. The average *z* scores in the region of interest decreased by 30% for 3D-SSP as the fc increased. The largest decrease in the *z* score in response to an increase in the fc was 14% for eZIS.

Detection Error

Figure 4 shows *z* score maps of hypoperfused regions on images generated at different fc settings. Table 2 shows changes in error between measured and prespecified areas of the hypoperfused region in response to changes in the fc of the Butterworth filter. When the normal database created at an fc of 0.50 cycles/cm (the same as that used for patient data creation) was analyzed using 3D-SSP, the hypoperfused region deviated from the actual value by 7.5%, which was the smallest error. When the normal database was generated at an fc of 0.40 cycles/cm, the error of the hypoperfused region increased to 40.2%. In contrast, the error dropped to 13.3% at an fc of 0.60 cycles/cm, resulting in underestimation.

The largest response to the variation in fc in the 3D-SSP analysis was a 50% shift. The error reached 55.3% in the eZIS analysis when processed using the normal database created at an fc of 0.50 cycles/cm (the same as that used for patient data creation). The maximum error was 70% in eZIS analysis when processed using a normal database created at a low fc. The error caused by changes in the fc was around 19% (Fig. 4).

Table 3 shows the result of changes in the volume of the region in response to the presence or absence of scatter and attenuation correction. The error of the hypoperfused region was reduced when scatter and attenuation were corrected in the normal databases and the patient data. This phenomenon was evident for both 3D-SSP and eZIS. Although still slightly underestimated, the error in the 3D-SSP analysis was as small as 3.3% when scatter was corrected and 2.15% when attenuation was corrected in the normal databases and the patient data. The error deviated from the actual value by 20% for 3D-SSP and 28% for eZIS when attenuation was corrected in the normal databases but not the patient data.

TABLE 1
Variation in Average *z* Scores in Region of Interest at Various Butterworth Filter fc Settings

Processing method	fc (cycles/cm)				
	0.4	0.45	0.5	0.55	0.6
3D-SSP	14.55	14.52	12.82	11.24	10.17
eZIS	14.2	13.91	13.51	12.83	12.24

DISCUSSION

The 3D-SSP and eZIS software packages are currently in wide use in nuclear medicine. These tools can accurately

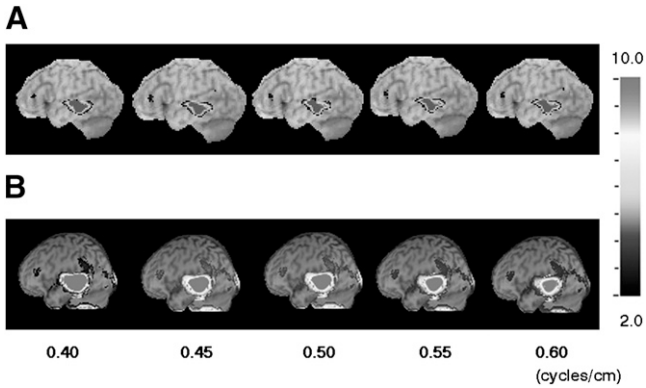

FIGURE 4. 3D-SSP (A) and eZIS (B) *z* score map images of left lateral brain surface when fc of Butterworth filter of normal database is changed while patient data remain constant. Pixel values are normalized to global brain, and images show decrease in *z* score. *z* score images confirm hypoperfused region. *z* score in each *z* score map image is scaled to 10.0 from 2.0.

TABLE 2
Error in Areas of Hypoperfused Region Compared with True Values

Processing method	fc of Butterworth filter (cycles/cm)				
	0.4	0.45	0.5	0.55	0.6
3D-SSP	40.21	25.65	7.51	−9.5	−13.33
eZIS	70.86	66.26	55.34	53.09	41.92

Units are % error of measured, compared with true, region size.

visualize slight changes in blood flow observed in dementia disease–related conditions such as Alzheimer disease and Lewy body disease. Hence, this method plays an extremely important role in disease stage classification and differential diagnosis (*6,7*). In contrast, because statistical imaging analysis evaluates the whole brain by voxels, the method can be objectively evaluated using images throughout the brain, including areas without predicted disease. Accordingly, we quantified SDs and reconstruction conditions (prefiltering, scatter correction, and attenuation correction) using normal databases and patient data.

The 3D-SSP analysis (Fig. 2A) shows that the SDs of the normal databases were significantly affected by the fc of the Butterworth filter. This type of filter is popular as a prefilter for reducing high-frequency noise in reconstructed images. The high-frequency component of the image is increased at a high fc in SPECT images. Therefore, when the fc of the Butterworth filter was increased, the images used for the normal databases probably included higher-frequency components that caused the peak of SD distribution of the normal databases to shift to higher values. The rate of change in the SD of the normal databases caused by variation in the fc reached 31% in the eZIS analysis; this value was relatively small compared with the largest percentage change observed in the 3D-SSP analysis.

The difference in the processing procedure between 3D-SSP and eZIS lies in smoothing after anatomic standardization. Image processing by eZIS is based on an SPM algorithm and uses a gaussian filter of 12 mm in full width at half maximum for smoothing after anatomic standardization. This smoothing process reduces differences between individual brains and effectively enhances the signal-to-noise ratio of images. Moreover, this smoothing process approximates the distribution of image pixel counts to normal—a prerequisite for statistical processing (*24*). However, image processing by 3D-SSP does not involve such a smoothing process. Therefore, the preanalysis image reconstruction conditions might affect the result. The process helped eZIS to reduce the magnitude of change in the SD scores of the normal databases in response to changes in fc. We consider that this smoothing process nullified the effects of the fc of the Butterworth filter for preprocessing.

Because z scores are determined by division with the SD of a normal database, it is expected that SD changes in a normal database will significantly affect the z score. Tables 1 and 2 show that z scores and the area of nonperfused brain tissue changed in response to changes in the SD distribution of the normal database. The volume of the nonperfused brain was accurately reproduced in the 3D-SSP analysis, with an error that was 1.1-fold the true volume when the Butterworth filters of the normal databases and patient data were set to the same fc. However, eZIS analysis overestimated the volume of the nonperfused brain, with an error that was 1.6-fold the true volume when the normal databases and the patient data were processed with the same fc. Ishitani et al. found that cerebral perfusion analysis using eZIS might evaluate the volume of nonperfused brain tissue as being 4- to 5-fold larger than its actual volume (*25*).

Shochiku et al. reported similar findings and suggested that the eZIS method overestimates perfusion defect (*26*). Thus, smoothing using a gaussian filter of 12 mm in full width at half maximum might significantly contribute to lesion size overestimation in eZIS analysis.

Figure 4 and Tables 1 and 2 indicate that smoothing decreases accuracy. Higher z scores, that is, a low SD of the normal database, are needed to improve the ability to detect abnormalities. In other words, sensitivity increases when the smoothing effect is higher, but the drawback is that accuracy is essentially reduced. These results suggest that automated processing should be investigated in more detail to minimize errors in clinical diagnoses.

The SDs significantly differed between normal databases corrected for scatter and those not corrected for scatter but not between those corrected and those not corrected for attenuation. Because scatter correction is deduced from scatter components collected from projection data, the

TABLE 3
Evaluation of Error of Hypoperfused Region According to Differences Between Compensation Methods

Processing method	NDB−, PD−		NDB+, PD+		NDB−, PD+		NDB+, PD−	
	AC	SC	AC	SC	AC	SC	AC	SC
3D-SSP	7.81	7.96	−2.15	−3.3	−13.54	19.27	−20.58	−19.79
eZIS	4.53	4.53	−4.12	−4.36	−13.17	10.7	−27.57	−23.87

Data are ratios. NDB− = without correction in normal database; PD− = without correction in patient data; NDB+ = with correction in normal database; PD+ = with correction in patient data.

signal-to-noise ratio of an image decreases after scatter correction. Therefore, scatter correction probably caused the SDs of the normal database to increase.

The scatter correction increased the average SD of the normal database by 27% and 30% for 3D-SSP and for eZIS, respectively. Furthermore, smoothing in the eZIS analysis decreased the SD of the normal database, compared with 3D-SSP, and the scatter correction resulted in no significant changes in the area of the nonperfused brain tissue relative to the fc. Smoothing using the gaussian filter reduced fluctuation in the average SD and consequently also reduced the fluctuation of the *z* score. These findings indicate that the accuracy of detecting nonperfused areas improves when scatter and attenuation are corrected in both the normal databases and patient data.

CONCLUSION

We quantified the effects of differences in SPECT image processing conditions (prefilter settings and scatter and attenuation correction) between normal databases and patient data using 2 statistical image analysis methods.

The image-processing conditions should be the same for normal databases and patient data in the 3D-SSP analysis because changes in the fc of the Butterworth filter and the presence or absence of scatter and attenuation correction during normal database creation significantly affect the SD of the normal databases. Smoothing using a gaussian filter of 12 mm in full width at half maximum might result in overestimation of the area of a nonperfused region in eZIS analysis, although percentage changes in the SD of normal databases and in the area of the nonperfused region would be small.

Therefore, the same image-processing conditions must be applied to normal databases and patient data in eZIS and 3D-SSP analyses. The accuracy of image analysis of brain function can be improved by correcting scatter and attenuation in both normal databases and patient data.

ACKNOWLEDGMENTS

No potential conflict of interest relevant to this article was reported.

REFERENCES

1. Camargo EE. Brain SPECT in neurology and psychiatry. *J Nucl Med.* 2001; 42:611–623.
2. Doody RS, Geldmacher DS, Gordon B, Perdomo CA, Pratt RD; Donepezil Study Group. Open-label multicenter, phase 3 extension study of the safety and efficacy of donepezil in patients with Alzheimer disease. *Arch Neurol.* 2001;58:427–433.
3. Winblad B, Engedal K, Soininen H, et al. A 1-year, randomized, placebo-controlled study of donepezil in patients with mild to moderate AD. *Neurology.* 2001;57:489–495.
4. Minoshima S, Giordani B, Berent S, Frey KA, Foster NL, Kuhl DE. Metabolic reduction in the posterior cingulate cortex in very early Alzheimer's disease. *Ann Neurol.* 1997;42:85–94.
5. Kogure D, Matsuda H, Ohnishi T, et al. Longitudinal evaluation of early Alzheimer's disease using brain perfusion SPECT. *J Nucl Med.* 2000;41:1155–1162.
6. Ishii K, Imamura T, Sasaki M, et al. Regional cerebral glucose metabolism in dementia with Lewy bodies and Alzheimer's disease. *Neurology.* 1998;51: 125–130.
7. Imon Y, Matsuda H, Ogawa M, Kogure D, Sunohara N. SPECT image analysis using statistical parametric mapping in patients with Parkinson's disease. *J Nucl Med.* 1999;40:1583–1589.
8. Ishii K, Sakamoto S, Sasaki M, et al. Cerebral glucose metabolism in patients with frontotemporal dementia. *J Nucl Med.* 1998;39:1875–1878.
9. Fox PT, Perimutter JS, Raichle ME. A stereotactic method of anatomical localization for positron emission tomography. *J Comput Assist Tomogr.* 1985;9:141–153.
10. Minoshima S, Foster NL, Kuhl DE. Posterior cingulate cortex in Alzheimer's disease [letter]. *Lancet.* 1994;344:895.
11. Minoshima S, Frey KA, Koeppe RA, Foster NL, Kuhl DE. A diagnostic approach in Alzheimer's disease using three-dimensional stereotactic surface projections of fluorine-18-FDG PET. *J Nucl Med.* 1995;36:1238–1248.
12. Bartenstein P, Minoshima S, Hirsch C, et al. Quantitative assessment of cerebral blood flow in patients with Alzheimer's disease by SPECT. *J Nucl Med.* 1997; 38:1095–1101.
13. Matsuda H, Mizumura S, Soma T, Takemura N. Conversion of brain SPECT images between different collimators and reconstruction processes for analysis using statistical parametric mapping. *Nucl Med Commun.* 2004;25: 67–74.
14. Mizumura S, Kumita S. Stereotactic statistical imaging analysis of the brain using the easy Z-score imaging system for sharing a normal database. *Radiat Med.* 2006;24:545–552.
15. Fox PT, Mintun MA, Reiman EM, Raichle ME. Enhanced detection of focal brain response using intersubject averaging and change distribution analysis of subtracted PET images. *J Cereb Blood Flow Metab.* 1988;8:642–652.
16. Lobaugh NJ, Caldwel CB, Black SE, Leibovitch FS, Swartz RH. Three brain SPET region-of-interest templates in elderly people: normative values, hemispheric asymmetries, and a comparison of single- and multihead cameras. *J Nucl Med.* 2000;41:45–56.
17. Ribeiro MJ, Remy P, Bendriem B, et al. Comparison of clinical data sets acquired on different tomography using 6-^{18}F-L-DOPA. *Eur J Nucl Med.* 2000;27: 707–712.
18. Van Laere K, Koole M, Versijpt J, et al. Transfer of normal ^{99m}Tc-ECD SPET database between different gamma cameras. *Eur J Nucl Med.* 2001;28:435–449.
19. Matsuda H, Mizumura S, Nagao T, et al. Automated discrimination between very early Alzheimer's disease and controls using an easy Z-score imaging system for multicenter brain perfusion SPECT. *Am J Neuroradiol.* 2007; 28:731–736.
20. Ogawa K, Harata Y, Ichihara T, Kubo A, Hashimoto A. A practical method for position-dependent Compton-scatter correction in single photon emission CT. *IEEE Trans Med Imaging.* 1991;10:408–412.
21. Ichihara T, Ogawa K, Motomura N, et al. Compton scatter compensation using the triple energy window method for single and dual isotope SPECT. *J Nucl Med.* 1993;34:2216–2221.
22. Beekman FJ, Kamphuis C, Frey EC. Scatter compensation methods in 3D iterative SPECT reconstruction: a simulation study. *Phys Med Biol.* 1997; 42:1619–1632.
23. Kadrmas DJ, Frey EC, Tsui BMW. Application of reconstruction based scatter compensation to thallium-201 SPECT: implementations for reduced reconstruction image noise. *IEEE Trans Med Imaging.* 1998;17:325–333.
24. Frackowiak R, Friston K, Frith C, et al. Analyzing brain image: principles and overview. San Diego, CA: Academic Press USA; 1997:25–41.
25. Ishigai N, Takahashi K, Tsuchiya F, Shiraishi M, Mochizuki A, Maruyama Y. Fundamental verification of extent threshold with eZIS [in Japanese]. *Nihon Kakuigakugijyutu Gaxtukai Zashi* 2003;23:507–510.
26. Matsutake Y, Onishi H. Influence of smoothing process on statistical brain function image analysis [in Japanese]. *Nippon Hoshasen Gijutsu Gakkai Zasshi.* 2008;64:426–433.